Interphase analysis of hierarchical composites via transmission electron microscopy

B. E. B. Uribe & J. R. Tarpani

Taylor & Francis
Taylor & Francis Group

Interphase analysis of hierarchical composites via transmission electron microscopy

B. E. B. Uribe ⓘ and J. R. Tarpani ⓘ

Department of Materials Engineering, São Carlos School of Engineering, University of São Paulo, São Carlos, Brazil

ABSTRACT

Observation and analysis of the interphase are essential for a detailed understanding of the global composite properties when nanofillers are incorporated as interfacial agents. Techniques such as atomic force microscopy and nano-indentation provide valuable information on interfacial properties associated with the viscoelastic behavior of each phase. However, when the morphology of this region is observed in detail, instrumental errors may regularly appear, decreasing the accuracy of measurements. In this work, the use of transmission electron microscopy (TEM) was explored to image the glass fiber-reinforced polymer GFRP interphase containing interfacial nanocellulose. TEM lamellas were prepared via a focused ion beam to observe the phases disposed within the composite arrangement. Energy dispersive X-ray spectroscopy was also performed to determine the elemental composition in each sample phase. Interphase sizes between 25 and 50 nm thick were found, highlighting the ability of this characterization route to give accurate interfacial measurements. This kind of measurement will open new routes for getting rich information on hierarchically structured composites containing a nanostructure as an interfacial agent.

Introduction

The concept of boundary layers or 'interphases' was first defined by Sharpe from Bell laboratories in 1972, as an excellent approach to understanding the mechanical behavior of adhesive joints [1]. Although this concept was originally associated to coatings and adhesives, it was later introduced in the field of polymer composites by Manson et al. [2] and Ishida et al. [3], with research focused directly on particle and fiber-reinforced plastics (i.e., glass/epoxy).

Meanwhile, the interface is responsible for the boundary between adherend and adhesive, the interphase is defined as a finite volumetric region, comprised of different links between the matrix and reinforcement with properties different from those of either one of the homogenous phases [4]. This important region is dominant in the mechanical and

---

physical properties of the macroscopic polymer composite, including volume expansion and shrinkage, transfer of stress and thermal stability [4–6].

Different techniques have been employed in the last decades to determine the main characteristics of this important region with a focus on its morphology, chemical adhesion, mechanical entanglement, and viscoelasticity among others. These diverse approaches are appropriate for the understanding of the interfacial dynamics in nano – and micro – levels, with the consequence of possible variations in interphase width, depending on the selected technique.

From a chemical perspective, the formation of the interphase/interface was successfully analyzed through spectroscopic techniques by different authors in the decades of 70s and 80s, providing valuable information in terms of molecular and microstructural variations of this region in composites, coatings and adhesive joints [3,7,8]. These works were essential to the understanding of the chemical reactions provided by coupling agents at the glass/epoxy interphase, which were demonstrated by means of Fourier transform infrared spectroscopy (FT-IR) [9–11]. Other studies reported values of interfacial widths measurements ranging from hundred nanometers [12,13] to several microns [14] in polymer composites using FT-IR spectroscopy.

Alternative approaches are based on nanohardness and nanoscratch tests to recognize the transition region between the main composite phases [15–18]. Different parameters such as hardness and the friction coefficient of the matrix in different positions close to the fiber were associated with transition zone values by 2 and 6 μm concerning to GF/polyester and to GF/phenolic composites, respectively. In another investigation, the influence of the type and concentration of silane coupling agents were observed in the interphase size of GF/vinylester, resulting in values varying between 0.8 and 1.5 μm from nanoindentation/ nanoscratch tests [19]. Although these techniques have been used to image the interphase even at nanoscale, they have been discussed because of the possibility of measuring artifacts rather than variations in the mechanical properties of the matrix [20].

The difference in stiffness between the composite phases has been also observed by atomic force microscopy (AFM). Studies such as those conducted by Griswold et al. [21] demonstrated that the proximity of fiber clearly affects the small size interphase (~210 nm) properties when the region is nano-indented; however, another perspective claimed that this transitional zone is a consequence of the local constrained polymer matrix in the fiber's vicinity [22]. Belec et al. studied the effects of different ageing conditions of GF/Epoxy composites revealing an interphase width of up to 500 nm width by using atomic force measurements [23]. One interesting route was presented by Gu et al. [24] after developing an interfacial assessment through the nanoscale dynamic mechanical imaging technique (nanoDMA), disclosing a ~100 nm interphase width by analyzing the variation of storage modulus of epoxy resin near to carbon fiber reinforcement. Similarly, Li et al. [25] found interphase thicknesses ranging from 80 to 270 nm by modulus mapping techniques when combined with scanning probe microscopy (SPM). Recently, studies such as that introduced by Wu et al. [26] used the transmission electron microscopy (TEM) technique to define a 200 nm interphase width in biphasic carbon/epoxy polymer composites previously prepared by a focused ion beam (FIB), ion etching and ultramicrotomy.

It is worth mentioning that there is little information concerning interphase measurements in composites with hierarchical structures (i.e., containing a nanometric substructure). For instance, the interphase width was found to be close to 200 nm by introducing

microfibrillated cellulose (MFC) as an interfacial agent in glass/epoxy (GFRP) composite laminates [27]. This study illustrates the influenced matrix at the surrounding interphase through an analysis of the viscoelastic variations between phases via AFM. Likewise, a modulus mapping [28] was envisioned to identify the interfacial characteristics of hierarchical glass fiber-reinforced poly (ether-ether ketone) containing carbon nanotubes as the substructure [15]. Nevertheless, the morphology, orientation, and size of the deposited nanostructure within the hierarchical composites have not been clearly illustrated.

In this research, we investigate in detail the interphase in hierarchical GFRP composites containing a nanocellulose substructure, using scanning transmission electron microscopy (STEM) techniques [29,30]. These results provide rich information concerning the shape, distribution and size of this nanostructure when deposited as an interfacial agent. Thus, the physical-mechanical properties of hierarchical composites may be understood from another useful perspective, likely by considering the use of combined techniques that allow a global comprehension of each type of material.

Materials and methods

Continuous unsized glass fiber (GF) in the form of 0/90 bidirectional plain-weave fiber fabric, supplied by Fibertex˙, displaying an areal weight of 200 g/m² was used as the main reinforcement. A liquid system composed of Araldite LY 1316-2 BR epoxy resin based on bisphenol A diglycidyl ether (DGEBA) monomer and Aradur HY 2963 based on cycloaliphatic amine hardener was purchased from Huntsman, Brazil. The nanocellulose in sugar cane bagasse was synthesized following the process described elsewhere [31], while TEMPO-oxidized cellulose nanofibers (TOCNs) were prepared according to Saito and Isogai [32]. Differences in size and morphology of these cellulose derivatives are illustrated in Figure 1.

Compounding unsized CF and GF fabrics with nanocellulose substructure (NC)

Neat GF fabrics were dipped in aqueous suspensions containing MFC and TOCNs with a 0.1 wt.% concentration, respectively. The impregnated fabrics were subsequently dried in an oven for 3 h at 102 ± 3 °C until the weight loss was negligible. Resin infusion under flexible tooling was employed to permeate dry preforms of hierarchical laminates [33]. Typically, the time spent on infusing each composite plaque was 3 h, giving rise in both cases to 1.0 mm-thick laminates. Subsequently, a fracture surface was produced in both composite systems to expose the nanocellulose-rich resin zones.

Characterization

FIB was performed in a FEI Helios 650 dual beam FIB-scanning electron microscope (SEM) instrument, with the Ga⁺ ions source at 30 KV. To prepare the TEM lamellas, a 10 μm platinum (Pt) protective layer was deposited onto each carbon and glass fiber surface containing a homogenous TOCNs coating. Lamellas were prepared in a range of 40–100 nm thickness until they were electron transparent for TEM analyses.

TEM studies were performed in an FEI Titan Low-Base microscope working at 80 kV and equipped with a CESCOR Cs probe corrector, an ultra-bright X-FEG electron source,
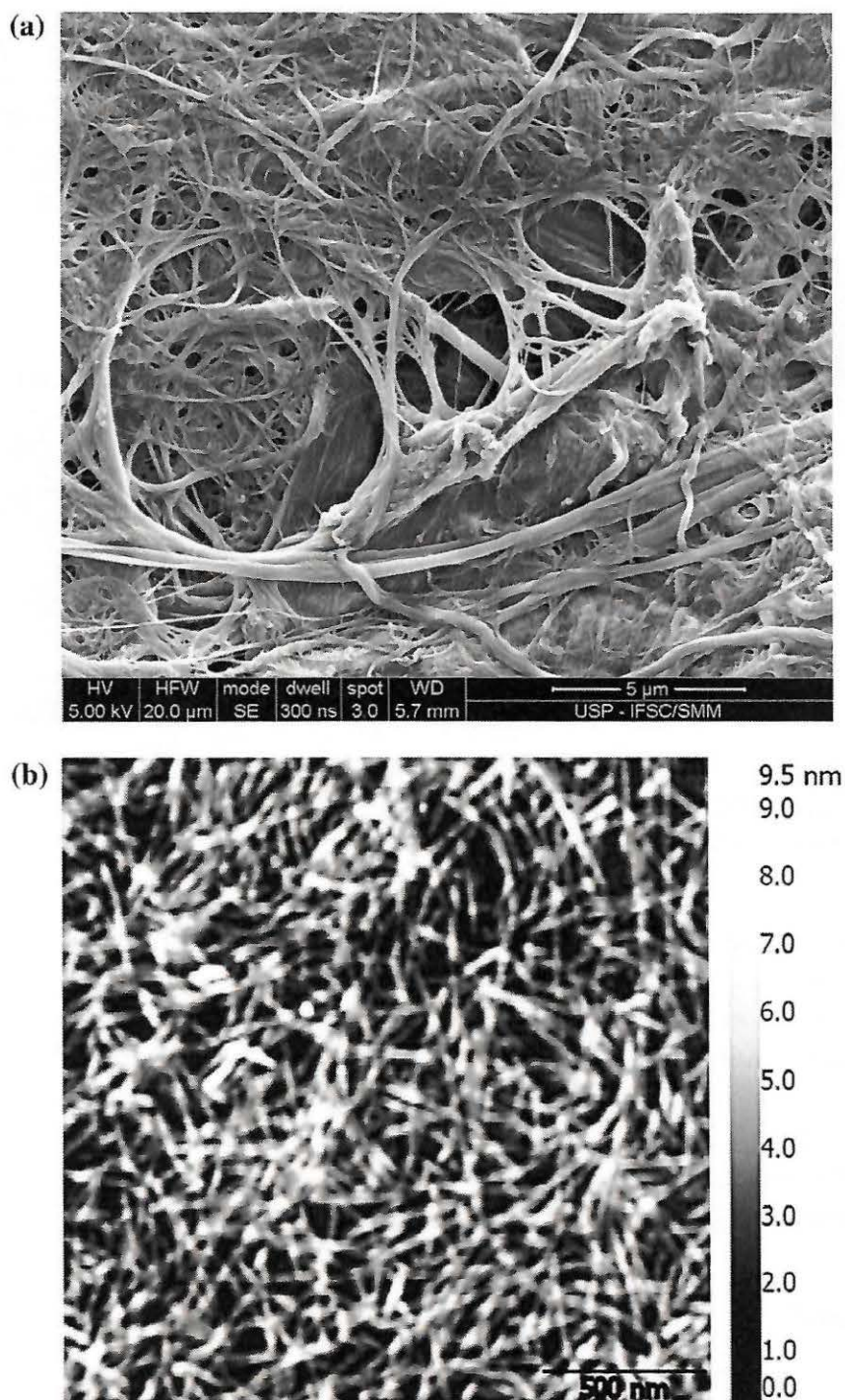
Figure 1. (a) SEM micrograph of MFC; (b) height AFM micrograph of TOCNs.

a monochromator and an energy-dispersive X-ray spectroscopy (EDS) detector. STEM imaging was performed by using a high-angle annular dark field (HAADF) detector.

Results and discussion

TEM sample preparation

Both GFRP-MFC and GFRP-TOCNs samples were observed using the FIB-SEM to determine the nanocellulose-rich resin zones onto each composite sample (C in Figure 2(a)).
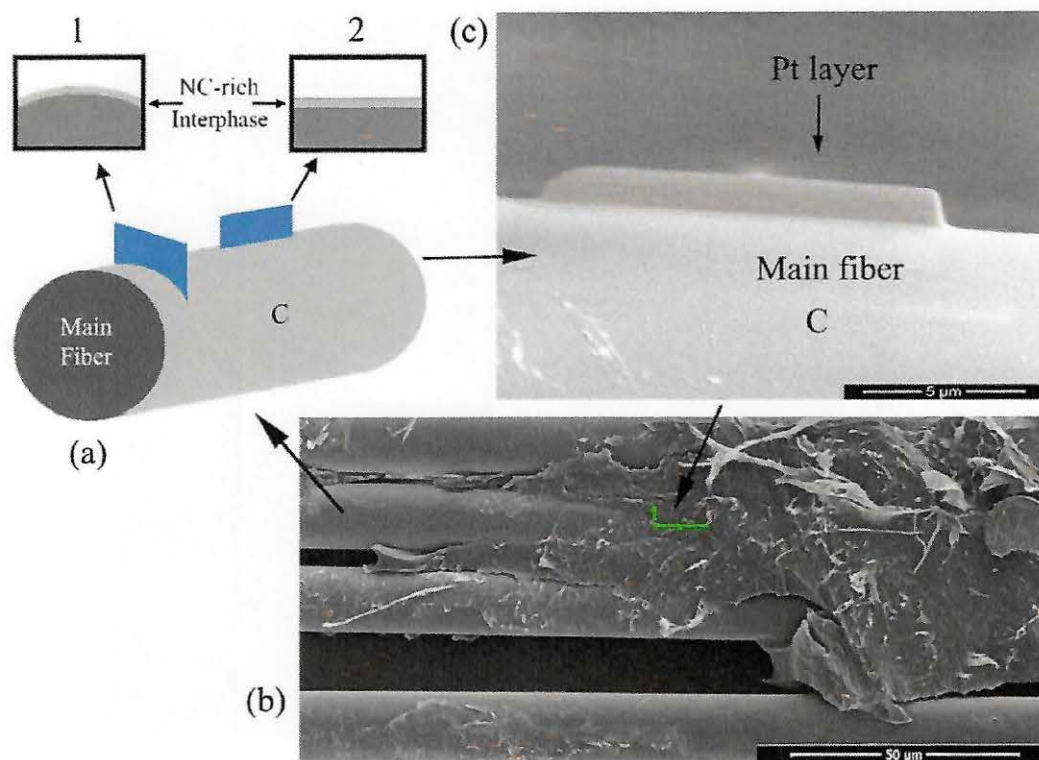
Figure 2. Scheme of FIB lamella preparation displaying (a) appropriate direction of lamella, (b) SEM micrograph of hierarchical surface, and (c) SEM image presenting the Pt protective layer.

Subsequently, an exposed single fiber containing nanocellulose was chosen, maintaining its axial direction as a main reference (Figure 2(b)–(c)). This convention was used to observe a linear interphase as indicated with number 2 in Figure 2(a), avoiding possible distortions associated with a more complex geometry (number 1, Figure 2(a)), where the nanocellulose deposition could be heterogeneous due to the shape factor. The standard FIB TEM-lamella procedure, see Suppl. Info., has been performed. A thicker region at the bottom of the sample has been left to avoid shrinkage deformations, which is a condition that is regularly observed in samples prepared by ultramicrotomy or ion beam etching [17,26,27].

STEM imaging

High-angle annular dark-field (HAADF) STEM micrographs were obtained to analyze the physical appearance of the fiber surrounding interphase based on the differences in atomic weight of the elements. Different parameters such as morphology, layer arrangements, nanostructure sizes and the elemental composition of phases were studied on each sample. Figure 3(a) clearly reveals the interphase comprised for MFC deposited onto the main glass fiber, while Figure 3(b) displays the TOCNs interfacial agent under the same latter considerations. For each micrograph, three different zones designate the principal regions of the lamella. Number '1' represents the thin layer of Pt deposited onto each surface to enhance the sample electronic conduction and to protect the sample during the lamella preparation, number '2' points out the nanocellulose-rich resin interphase, and number '3' is denoted the main glass fiber reinforcement. In Figure 3(a), several nanofibers (indicated with black arrows) are observed presenting different widths between 12 and 15 nm. These
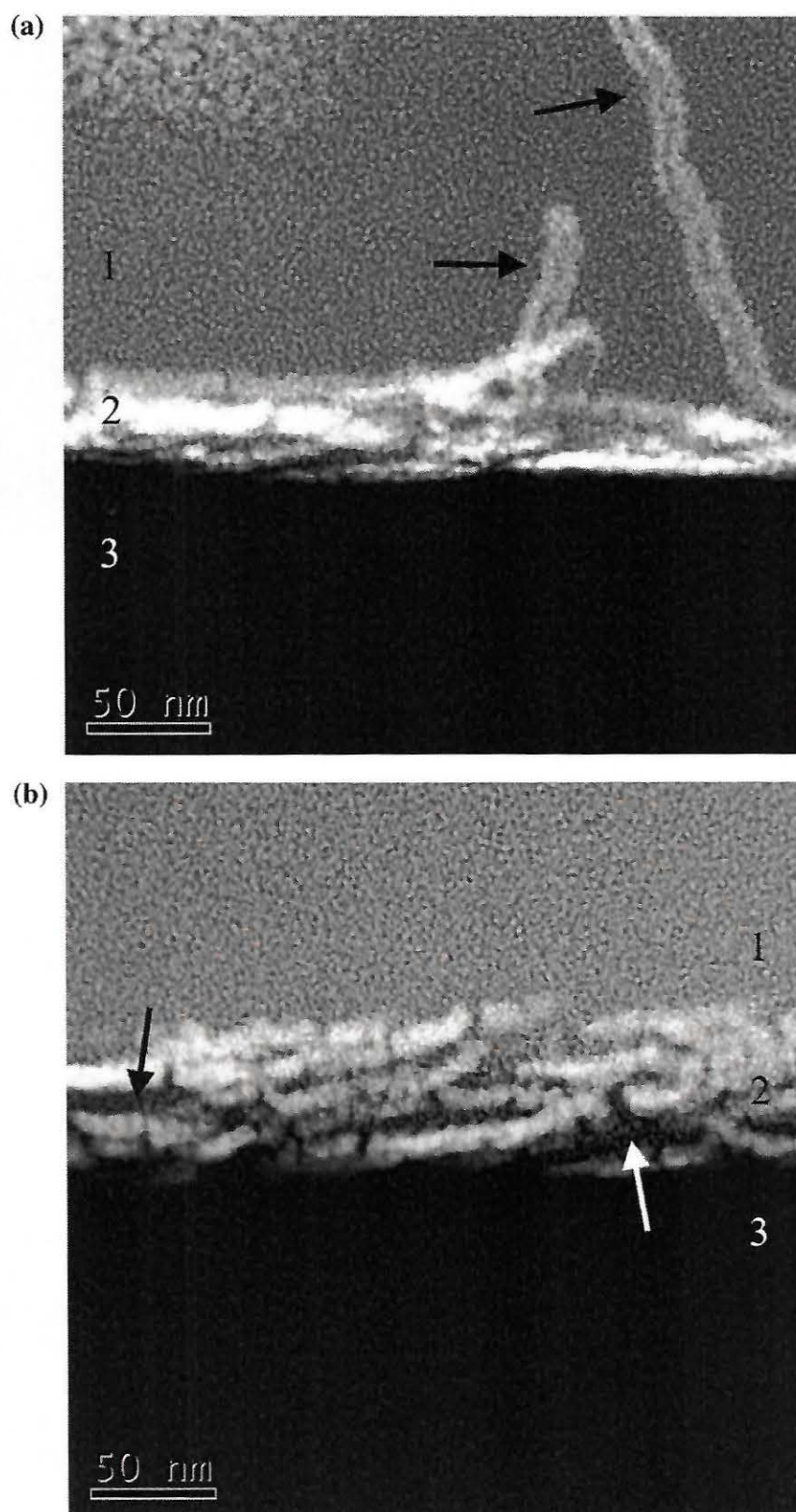
Figure 3. HAADF STEM micrographs displaying matrix/fiber interphase respectively in (a) GFRP+MFC; (b) GFRP+TOCNs.
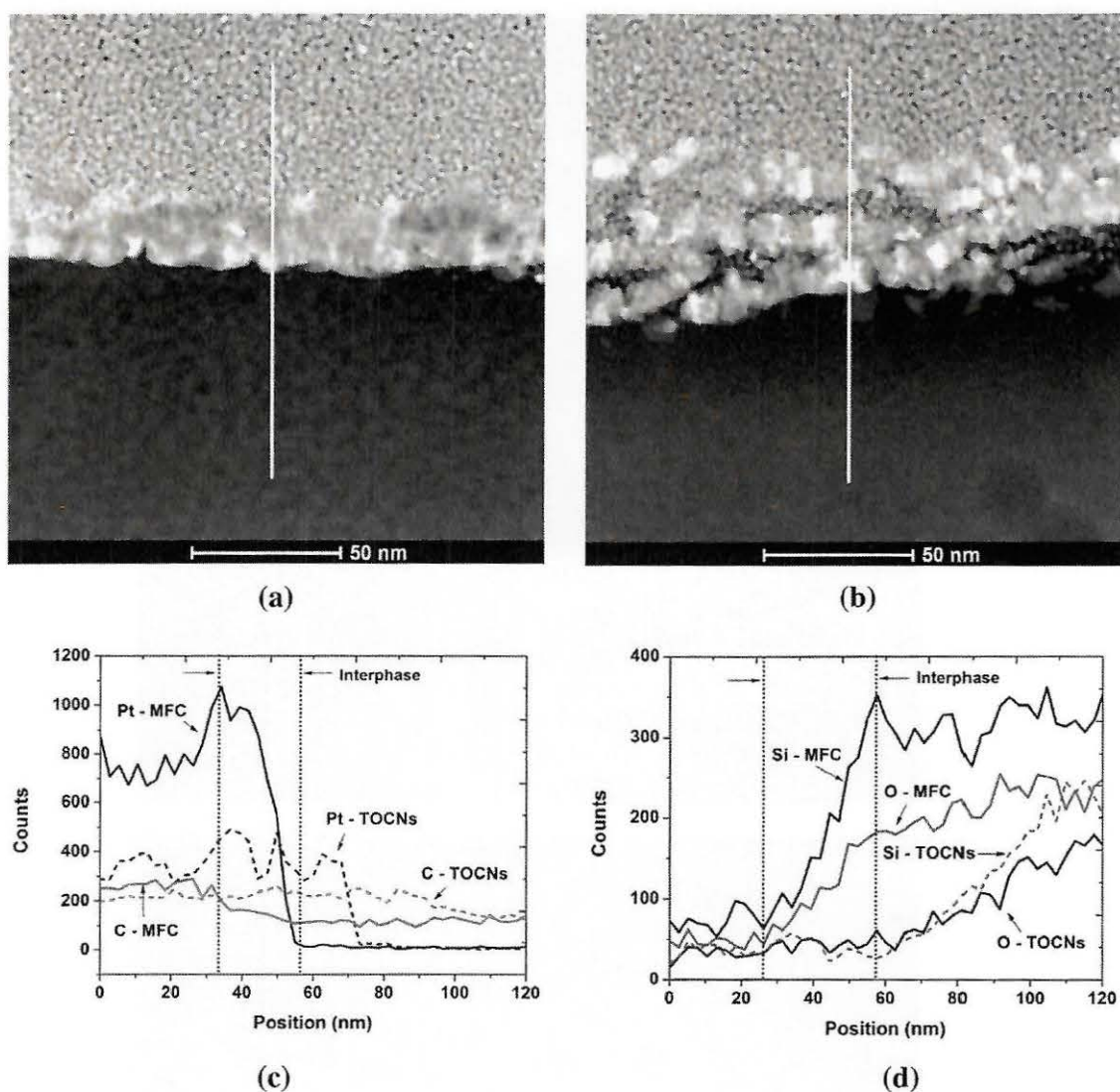
Figure 4. EDS-STEM analysis displaying (a) GFRP-MFC and (b) GFRP-TOCNs spectrum line acquisition regions; the spectra of (c) Pt and C elements; (d) Si and O elements of GFRP-MFC and GFRP-TOCNs composites.

nanofibers are aligned in out-of-plane directions that correspond to the interlaminar region within the composite fabrics. This arrangement provides reinforcement of the matrix in the interfacial neighborhood through the cellulose nanobridges, improving properties such as delamination resistance and shear stress in the hierarchical structure of the composite laminate [6,34,35]. Figure 3(a) also shows a thinner MFC interphase of 25–40 nm thick likely with the presence of some MFC fibrils, displaying a resin-rich region that prevents the observation of single MFC units indicating that the resin system successfully impregnated the nanofiber mesh (Figure 1(a)).

Figure 3(b) displays a micrograph of a composite interphase comprised of GFRP-TOCNs. This cellulosic material is different when compared to MFC because its synthesis route results in an oxidized structure with repulsive charges at its surface [36,37]. Therefore, a region characterized by separation between fibers is expected, as denoted with arrows in Figure 3(b). In contrast to MFC interphase, TOCNs present a structure without resin

permeation during the manufacturing process, likely associated with the resin viscosity apparently high enough to percolate the tiny mesh of TOCNs (Figure 1(b)). Isolated nano-fibers ranging from 6 to 10 nm wide (Figure 1(b)) were also measured in Figure 3(b), corroborating the presence of an organized and homogenous structure. The overall interphase width of TOCNs including resin-free spaces was also measured in Figure 3(b), resulting in sizes from 35 to 50 nm.

In order to characterize the elemental composition on both GFRP-MFC and GFRP-TOCN samples, we developed EDS-STEM analyses [21]. An excellent example of EDS linear scanning at the interphase from matrix to reinforcement is presented by Li et al [38]. In the recorded spectrum-lines, Figure 4(c)–(d) [39,40] extracted from regions denoted with vertical white lines on Figure 4(a)–(b) respectively, it was observed that carbon presented a minimal decreasing trend in both composite laminates when measured from the Pt zone to GF reinforcement. Unlike the composite lamella containing TOCNs, the carbon content in the MFC composite interphase was associated with the remaining epoxy resin in this region due to the favorable impregnation during composite manufacturing. On the other hand, atomic contents in carbon and oxygen elements (main nanocellulose and epoxy constituents) are not high enough representative in this class of materials to give accurate information regarding phase differences. It implies that when carbon or oxygen are detected in the interfacial region, the signal may be produced by both resin and nanocellulose phases without any contrasting advantage that enables their isolated identification – a fact that suggests the use of staining methods to change the contrast of at least one phase (e.g., nanocellulose) due to the incorporation of heavy atoms within its structure. This limitation was not observed for platinum and silicon elemental distribution, recalling that Pt is an element that is deposited during the surface metallization of the sample [30], while Si as well as oxygen are the main elements of glass fiber reinforcement [6]. Figure 4(c)–(d) show a clear distribution of these elements, respectively, starting at the Pt-rich surface, crossing the nanocellulose interphase and finishing at the main glass fiber. As expected, Pt decreased its signal as it went deep in the sample. In contrast, the silicon amount increases at the last part of the spectrum-line, indicating the presence of the glass fiber. Vertical dashed lines in Figure 4(c)–(d) denote the transitional zone (interphase) measured directly from Pt and Si signals, respectively extracted from GFRP-MFC curves. The resulting interphase values between 25 and 30 nm corroborating HRSTEM images (Figures 3(a) and 4(a)). The measurement was performed only to GFRP-MFC composites because a thick and sealed interphase structure was previously observed, preventing mass transfer of Pt and Si elements through the nanocellulose mesh. This behavior contrasted with that observed in GFRP-TOCNs composites where resin-free areas with sizes between 5 and 8 nm were found to hamper the accuracy of EDS in the interphase measurement.

When the interphase width is measured in detail it is important to clarify that each of the techniques employed may be sensitive to different parameters such as viscoelastic response, chemical structure, and electrical charges, among others; which can provide different results even in the same sample. Taking this into account, the use of combined characterization techniques could be a reliable alternative for understanding the global properties of the interphase in this novel class of hierarchical polymer composites.

Conclusion

A clear assessment and precise measurement of the interphase in GFRP containing microfibrillated cellulose and TEMPO-oxidized cellulose nanofibers were successfully obtained and demonstrated by means of the current methodology. We have proved that FIB is the most appropriate method for TEM lamella preparation for these materials. This preparation method limits/prevents the deformation of the interphases of these samples composed by flat surfaces and allows a perfect microstructural investigation. The combination of HRSTEM and EDS was conclusive and determined the main features of the interphase such as shape, orientation of fibers and sizes, resulting in values between 25 and 40 nm and 35 and 50 nm width for GFRP-MFC and GFRP-TOCNs composites, respectively. The isolated nanofibers were also estimated between 12–15 nm, and 6–10 nm wide, for the former and the latter hierarchical composite systems, respectively. These results demonstrate great potential of these techniques to give accurate interfacial information at the nanoscale. Thus, these works effectively contribute to the analysis of interphases in polymer composites containing a nanostructure as an interfacial agent.

Disclosure statement

No potential conflict of interest was reported by the authors.

ORCID

B. E. B. Uribe http://orcid.org/0000-0002-7229-0874
J. R. Tarpani http://orcid.org/0000-0003-1201-8999

References

[1] Sharpe LH. The interphase in adhesion. J Adhes. 1972;4:51–64.
[2] Manson JA, Sperling LH. Polymer blends and composites. Boston (MA): Springer; 1976.
[3] Ishida H, Koenig JL. The reinforcement mechanism of fiber-glass reinforced plastics under wet conditions: a review. Polym Eng Sci. 1978;18:128–145.
[4] Miller JD, Ishida H. Adhesive – adherend interface and interphase BT – fundamentals of adhesion. In: Lee L-H, editor. Boston (MA): Springer; 1991. p. 291–324.
[5] Jancar J. Review of the role of the interphase in the control of composite performance on micro- and nano-length scales. J Mater Sci. 2008;43:6747–6757.
[6] Karger-Kocsis J, Mahmood H, Pegoretti A. Recent advances in fiber/matrix interphase engineering for polymer composites. Prog Mater Sci. 2015;73:1–43.

[7] Ishida H. A review of recent progress in the studies of molecular and microstructure of coupling agents and their functions in composites, coatings and adhesive joints. Polym Compos. 1984;5:101–123.

[8] Ishida H, Koenig JL. Fourier transform infrared spectroscopic study of the silane coupling agent/porous silica interface. J Colloid Interface Sci. 1978;64:555–564.

[9] Culler SR, Ishida H, Koenig JL. Nondestructive FT-IR sampling technique to study glass fiber composite interfaces. Appl Spectrosc. 1984;38:1–7.

[10] Culler SR, Ishida H, Koenig JL. FT-IR characterization of the reaction at the silane/matrix resin interphase of composite materials. J Colloid Interface Sci. 1986;109:1–10.

[11] Hoh K-P, Ishida H, Koenig JL. Spectroscopic studies of the gradient in the silane coupling agent/matrix interface in fiberglass-reinforced epoxy. Polym Compos. 1988;9:151–157.

[12] Garton A. FT-IR of reinforced plastics. Proceedings SPIE 0553. Fourier and computerized infrared spectroscopy; 1985 Dec 20; Ottawa; 1985. p. 190–191.

[13] Garton A, Daly JH. Characterization of the aramid: epoxy and carbon: epoxy interphases. Polym Compos. 1985;6:195–200.

[14] Ikuta N, Yanagawa A, Suzuki Y, et al. Investigation of resin interphase produced near silane-treated glass fiber in vinyl ester resin. Compos Interfaces. 2001;7:511–515.

[15] Díez-Pascual AM, Gómez-Fatou MA, Ania F, et al. Nanoindentation assessment of the interphase in carbon nanotube-based hierarchical composites. J Phys Chem C. 2012;116:24193–24200.

[16] Hodzic A, Stachurski ZH, Kim JK. Nano-indentation of polymer – glass interfaces part I. Experimental and mechanical analysis. Polymer. 2000;41:6895–6905.

[17] Hodzic A, Kim JK, Stachurski ZH. Nano-indentation and nano-scratch of polymer glass interfaces II model of interphases in water. Polymer. 2001;42:5701–5710.

[18] Hodzic A, Kalyanasundaram S, Kim JK, et al. Application of nano-indentation, nano-scratch and single fibre tests in investigation of interphases in composite materials. Micron. 2001;32:765–775.

[19] Kim J-K, Sham M-L, Wu J. Nanoscale characterisation of interphase in silane treated glass fibre composites. Compos Part A Appl Sci Manuf. 2001;32:607–618.

[20] Young TJ, Monclus M, Broughton WR, et al. Observations on interphase characterisation in polymer composites by nanoscale indentation and use of AFM cantilever torsion to identify measurement artefacts. Plast Rubber Compos. 2012;41:240–246.

[21] Griswold C, Cross WM, Kjerengtroen L, et al. Interphase variation in silane-treated glass-fiber-reinforced epoxy composites. J Adhes Sci Technol. 2005;19:279–290.

[22] Gohil PP, Shaikh AA. Analytical investigation and comparative assessment of interphase influence on elastic behavior of fiber reinforced composites. J Reinf Plast Compos. 2009;29:685–699.

[23] Belec L, Nguyen TH, Nguyen DL, et al. Comparative effects of humid tropical weathering and artificial ageing on a model composite properties from nano- to macro-scale. Compos Part A Appl Sci Manuf. 2015;68:235–241.

[24] Gu Y, Li M, Wang J, et al. Characterization of the interphase in carbon fiber/polymer composites using a nanoscale dynamic mechanical imaging technique. Carbon 2010;48:3229–3235.

[25] Li M, Wang J, Zhang Z, et al. Characterization of the interphase width in carbon fibre reinforced epoxy resin composites. Proceedings of the 17th ICCM. Edinburgh, United Kingdom. 2009. p. 1–8.

[26] Wu Q, Li M, Gu Y, et al. Imaging the interphase of carbon fiber composites using transmission electron microscopy: preparations by focused ion beam, ion beam etching, and ultramicrotomy. Chin J Aeronaut. 2015;28:1529–1538.

[27] Uribe BEB, Carvalho AJF, Tarpani JR. Low-cost, environmentally friendly route to produce glass fiber-reinforced polymer composites with microfibrillated cellulose interphase. J Appl Polym Sci. 2016;44183:1–9.

[28] Díez-Pascual AM, Gómez-Fatou MA, Ania F, et al. Nanoindentation in polymer nanocomposites. Prog Mater Sci. 2015;67:1–94.

[29] Langlois C, Benzo P, Arenal R, et al. Fully crystalline faceted Fe–Au core-shell nanoparticles. Nano Lett. 2015;15:5075–5080.

[30] Deepak FL, Mayoral A, Arenal R, editors. Advanced transmission electron microscopy. Cham: Springer International Publishing; 2015.

[31] Carvalho AJ. Nanocelluloses from eucalyptus wood pulp. J Renew Mater. 2014;2:118–122.
[32] Saito T, Nishiyama Y, Putaux J-L, et al. Homogeneous suspensions of individualized microfibrils from TEMPO-catalyzed oxidation of native cellulose. Biomacromolecules. 2006;7:1687–1691.
[33] Poorzeinolabedin M, Parnas L, Dashatan SH. Resin infusion under flexible tooling process and structural design optimization of the complex composite part. Mater Des. 2014;64:450–455.
[34] Uribe BEB, Chiromito EMS, Carvalho AJF, et al. Low-cost, environmentally friendly route for producing CFRP laminates with microfibrillated cellulose interphase. Express Polym Lett. 2017;11:47–59.
[35] Qian H, Greenhalgh ES, Shaffer MSP, et al. Carbon nanotube-based hierarchical composites: a review. J Mater Chem. 2010;20:4751–4762.
[36] Habibi Y, Chanzy H, Vignon MR. TEMPO-mediated surface oxidation of cellulose whiskers. Cellulose. 2006;13:679–687.
[37] Saito T, Kimura S, Nishiyama Y, et al. Cellulose nanofibers prepared by TEMPO-mediated oxidation of native cellulose. Biomacromolecules. 2007;8:2485–2491.
[38] Li ZK, Fu HM, Sha PF, et al. Atomic interaction mechanism for designing the interface of W/Zr-based bulk metallic glass composites. Sci Rep. 2015;5:8967.
[39] Jeanguillaume C, Colliex C. Spectrum-image: the next step in EELS digital acquisition and processing. Ultramicroscopy. 1989;28:252–257.
[40] Arenal R, de la Peña F, Stéphan O, et al. Extending the analysis of EELS spectrum-imaging data, from elemental to bond mapping in complex nanostructures. Ultramicroscopy. 2008;109:32–38.